



Green synthesis, crystal growth, and some physicochemical studies on an inter-molecular compound of anthranilic acid and *m*-nitrobenzoic acid system

U. S. Rai¹ · Manjeet Singh¹ · R. N. Rai¹

Received: 24 June 2017 / Accepted: 27 April 2018 / Published online: 15 May 2018
© Akadémiai Kiadó, Budapest, Hungary 2018

Abstract

The phase diagram of anthranilic acid (AA)–*m*-nitro benzoic acid (NBA) system, determined by the thaw–melt method, shows the formation of a 2:1 (AA:NBA) inter-molecular compound (IMC) and two eutectics E_1 and E_2 containing 0.084 and 0.917 mol fractions of AA, respectively, with one eutectic on either side of the IMC. The heat of mixing, entropy of fusion, roughness parameter, interfacial energy, and the excess thermodynamic functions were calculated from the enthalpy of fusion data, obtained by the DSC method. While the spectroscopic investigations (IR and NMR) and optical studies suggest the presence of hydrogen bonding between the components, the powder X-ray diffraction spectra of eutectics and the IMC suggest that the eutectic E_1 is a mechanical mixture of the IMC and NBA and the eutectic E_2 is a mechanical mixture of the IMC and AA. A single crystal of cocrystal of AA and NBA was grown using slow evaporation technique at room temperature from its saturated solution in methanol solvent. Single-crystal analysis of the grown cocrystal shows the mode of the intermolecular hydrogen bonding in the molecule and the triclinic crystal structure with $P - 1$ space group.

Keywords Phase diagram · Cocrystal · Heat of fusion · Emission spectra · Single-crystal growth

Introduction

In the modern age of science and technology, materials with diverse properties and low cost are required to cater the needs of current civilization. Low transformation temperature, ease of purification, transparency, wider choice of materials, and minimized convection effects are the special features which have prompted a large number of research workers [1–6] to use organic systems for detailed physicochemical investigations. Recently, organic materials have also been reported [2, 7] for various electronic and photoelectronic applications such as transistor, conductor, light-emitting diode, liquid crystal display, and nonlinear

optical materials. Horiuchi et al. [8, 9] have discovered a new class of organic materials in which cocrystals with non-covalent bonding form supramolecular structure, having a first-order ferroelectric phase transformation and high dielectric permittivity and resistivity. Abbott et al. [10] have found that eutectic mixtures of urea and a range of quaternary ammonium salts are liquid at ambient temperature and have interesting solvent properties. Organic eutectics and IMC have their potential applications in medicine and pharmaceutical industries [11, 12]. The role of crystallization and interaction between the molecules are well recognized for manufacturing of the advanced functional materials via the modification of physicochemical properties [13]. In addition, the parent compounds with acidic or phenolic and amine groups are found to show interesting interactions through non-covalent bondings [14] such as hydrogen bonding (O–H...O, O–H...N or N–H...O), dipole–dipole interaction, and dispersion forces. On the other hand, the parent components with acidic/phenolic and amine groups are found to be interesting for the interactions through hydrogen bonds in solid phase and have been found promising for crystal engineering [15, 16]. It is quite interesting that the physicochemical investigations show

Electronic supplementary material The online version of this article (<https://doi.org/10.1007/s10973-018-7344-2>) contains supplementary material, which is available to authorized users.

✉ U. S. Rai
usrai_bhu@yahoo.co.in

¹ Department of Chemistry, Centre of Advanced Study, Institute of Science, Banaras Hindu University, Varanasi 221005, India

intermolecular hydrogen bonds between the parent components and insist on the further investigation to synthesize novel materials by retaining their functional groups [17].

AA ($C_7H_7O_2N$) has so many industrial, biological, pharmaceutical applications as its esters are used in preparing perfumes to imitate jasmine and orange in addition to their use to generate benzyne [18]. In addition, NBA ($C_7H_5O_4N$) is a nitro group and a carboxylic group containing compound suitable for non-covalent bonding with the compound containing amino and hydroxyl groups. With a view to elucidate the chemistry of AA–NBA system and to prepare their eutectics and IMC without any solvent involving solid-state reaction, phase diagram of the system was studied to determine their composition and melting temperatures. The binary compounds were characterized by spectral, thermal, and X-ray diffraction methods. A single crystal of the convenient size as cocrystal was also grown by the solvent evaporation method at room temperature from its saturated solution in methanol solvent.

Experimental

Materials and their purification

The parent compounds, AA and NBA, received from Aldrich, Germany, were purified by repeated crystallization from methanol. The purity of each of AA and NBA compounds was ascertained by the determination of their melting temperatures which were found to be 147.0 and 140.0 °C, respectively. The melting points are quite close to their values reported in the literature [16].

Phase diagram

The phase diagram of AA–NBA system was determined by preparing the mixtures in the entire range of compositions, by weighing appropriate amount of each of AA and NBA using four-digit balance (Denver SI-234, Germany) of accuracy ± 0.0002 g. After sealing the mouth of each test tube to avoid the flight of molecules, these mixtures were homogenized by repeating the process of melting the mixture followed by chilling in ice-cold water. The process of melting and chilling was repeated five times to ensure complete homogenization. The melting points of these mixtures were determined using Toshniwal melting point apparatus attached to a thermometer with accuracy ± 0.5 °C [18]. The phase diagram of the system was determined by plotting graph between mole fraction of AA and NBA compounds on X-axis and their melting points on Y-axis.

Spectroscopic studies

FTIR spectra of the pure components and the IMC were recorded at 300 K in the region 4000–400 cm^{-1} using a Perkin Elmer FTIR Spectrum 1000 Infrared Spectrometer. The proton NMR spectra were also recorded in $CDCl_3$ by JEOL AL300 MHz spectrometer.

Enthalpy of fusion

The values of heat of fusion of the pure components, the eutectics, and the IMC were determined by DSC (Mettler DSC-4000). Indium and zinc samples were used to calibrate the DSC unit. The amount of test sample and heating rate were about 7 mg and 5 °C min^{-1} , respectively.

X-ray diffraction

Powder X-ray diffraction (XRD) patterns of the pure components, the eutectics, and the inter-molecular compound were recorded using an 18 kW rotating (Cu) anode-based Rigaku powder diffractometer fitted with a graphite monochromator in the diffracted beam. The samples were scanned from 10° to 70° with a scanning rate of 4°/min.

Study on single-crystal growth and atomic packing

To obtain its single crystal, we dissolve the synthesized novel IMC materials in methanol at room temperature to get its saturated solution. A single crystal of the cocrystal of AA–NBA was grown from the saturated methanol solution by slow evaporation technique. Single-crystal X-ray diffraction data were collected using the X Caliber Oxford CCD diffractometer. While the data reduction was carried out using Chrysalis Pro software, the structure solution and refinement were studied utilizing SHELXS and SHLEXL-97 [19].

Optical studies

The absorption spectra of pure compounds and the IMC were recorded using a UV/Vis/NIR (JASCO Model V-670) spectrometer from 190 to 700 nm at room temperature in methanol solution (1.0×10^{-5} M). Fluorescence spectra were also recorded on a Varian Cary eclipse fluorescence spectrophotometer using pyrene as reference at room temperature in the same solvent and identical concentration.

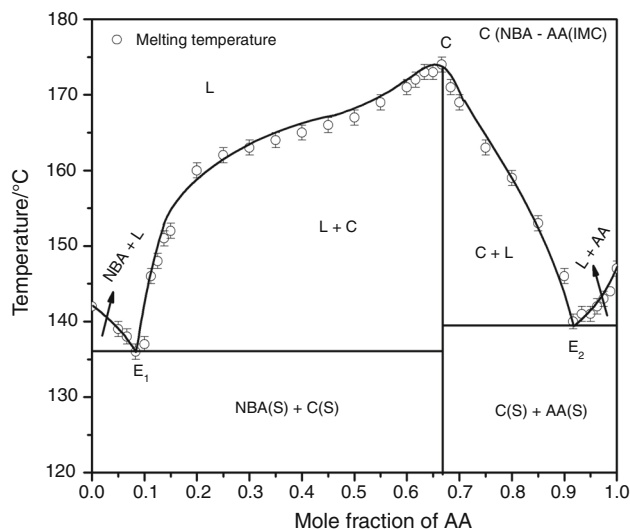


Fig. 1 Phase diagram of AA and NBA

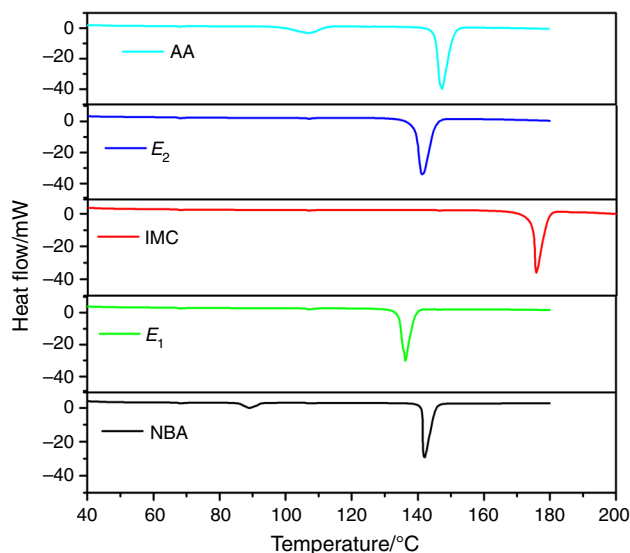
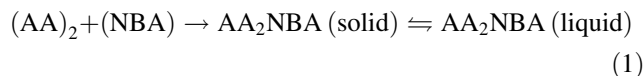


Fig. 2 DSC plots of AA, NBA, their eutectics, and the cocrystal

Results and discussion

Phase diagram

The phase diagram of the AA–NBA system shows the formation of a 2:1 (AA:NBA) inter-molecular compound (IMC) at point C having a congruent melting point and two eutectics E_1 and E_2 containing 0.084 and 0.917 mol fraction of AA, respectively. The melting points of E_1 , E_2 and the IMC are 136.0, 140.0, and 174.0 °C, respectively (Fig. 1). It is evident from this figure that the melting point of NBA decreases with the addition of the second component AA and it attains the minimum value (136.0 °C) at the first eutectic point E_1 . Further addition of AA causes the melting point to rise till it attains the maximum at C (174.0 °C) where the compositions of liquid and solid phases are identical. This maximum temperature is the congruent melting point of the IMC. Due to further increase in mole fraction of AA, the melting point of the mixtures decreases and it attains the minimum (140.0 °C) at the second eutectic point E_2 . The melting points of each mole fractions are given in supplementary data (Table S1). The existence of a maximum and eutectic points on either side of the maximum point imparts stability [20] to the IMC. The reaction between two components giving a congruent melting compound may be represented by equation:



In the liquid phase, the IMC (AA_2NBA) may remain either in dissociated or in the molecular form. If there is no dissociation in the IMC in the molten condition, the phase diagram would show a sharp maximum. However, when dissociation occurs in the molten state, the products of dissociation lower the effective mole fraction of the solute, and the curve would be flattened. For each eutectic, the IMC behaves as one of the components. The observed

Table 1 Enthalpy of fusion, heat of mixing, entropy of fusion, roughness parameters, and interfacial energy of pure components, their eutectics, and the IMC

S. no.	Materials	Enthalpy of fusion/kJ mol ⁻¹	Heat of mixing/kJ mol ⁻¹	Entropy of fusion/J mol ⁻¹ K ⁻¹	Roughness parameter/ α	Interfacial energy $\times 10^{-3}$ /J m ⁻²
1.	AA	24.72		58.90	7.08	48.49
2.	NBA	20.49		49.40	5.94	36.51
3.	Eutectic 1 (Exp.)	22.67	– 3.88	55.40	6.66	37.51
	(Cal.)	26.54				
4.	Eutectic 2 (Exp.)	30.26	– 5.49	73.30	8.82	47.49
	(Cal.)	35.75				
5.	IMC (Exp.)	68.87	45.56	15.34	18.45	44.50
	(Cal.)	23.31				

Table 2 Excess thermodynamic functions of eutectics of AA–NBA system

S.N.	Systems	$g^E/\text{kJ mol}^{-1}$	$h^E/\text{kJ mol}^{-1}$	$s^E/\text{kJ mol}^{-1} \text{K}^{-1}$
1	Eutectic 1	0.2547	10.3279	0.0246
2	Eutectic 2	0.2421	56.1572	0.1354

maximum in the system under investigation is flat indicating thereby that the IMC is capable of existing in solid in equilibrium with the liquid of the same composition.

Spectroscopic studies on the IMC

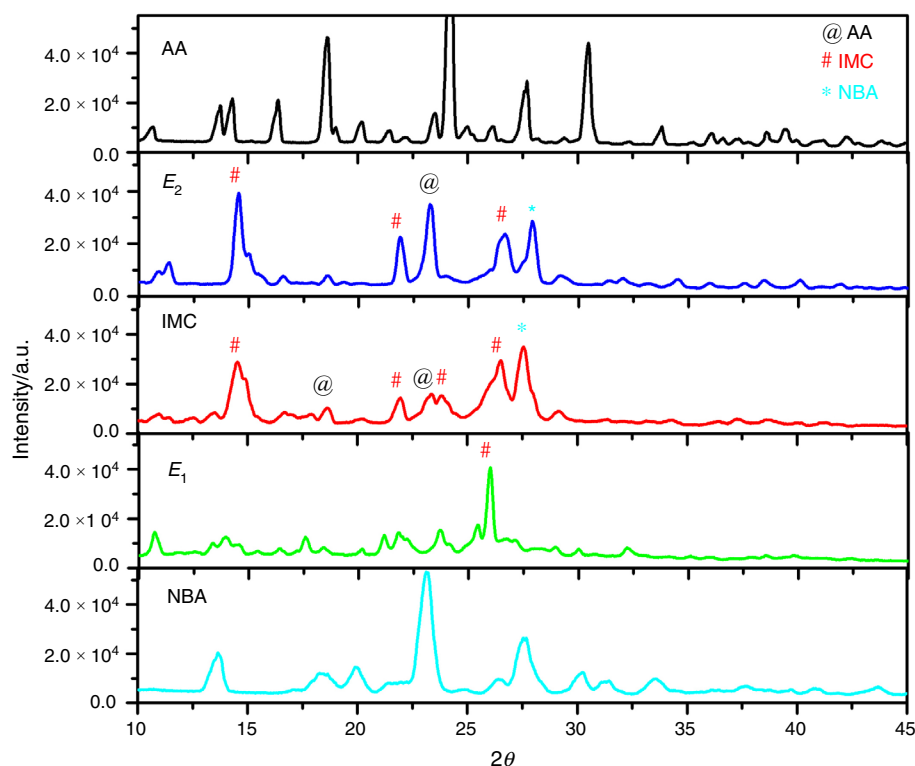
IR spectra

The peaks observed at 3086 and 1693 cm^{-1} in NBA spectrum (Fig. S1) are due to O–H and C=O stretching of carboxylic group (–COOH), respectively, and those at 1615, 1584, and 1415 cm^{-1} in the spectrum are indicative of aromatic –C=C– stretching frequencies. The peaks observed at 1531 and 1448 cm^{-1} in the spectrum of NBA are indicative of asymmetrical and symmetrical stretching frequency of nitro group. The peaks observed at 3325, 3240, 1677, and 1662 cm^{-1} in AA (Fig. S2) are due to N–H, O–H, and C=O stretching frequency of amine, hydroxy, and carbonyl of carboxylic groups, respectively. The peaks observed at 3489, 3379, 3094 cm^{-1} in the IMC spectrum

(Fig. S3) are due to stretching frequency of –O–H of carboxylic group of AA and NBA, respectively, and peaks at 1683 and 1560 cm^{-1} are due to C=O stretching frequency of the carboxylic group of the NBA and AA, respectively. The peaks observed at 1615, 1592, and 1486 cm^{-1} in the spectrum of IMC are indicative of aromatic –C=C– stretching frequencies. The peaks at 1521 and 1448 cm^{-1} in the spectrum of IMC are due to asymmetrical and symmetrical stretching frequency of nitro group. Shifting of –NH₂ frequency of AA and that of C=O frequency of NBA of –COOH suggest that there is intermolecular hydrogen bonding between AA and NBA.

NMR spectra

In ¹H NMR spectrum of NBA (Fig. S4), the peaks were observed at $\delta = 11.41$ ppm (1H s), 8.96 ppm (1H s), 8.48 ppm (1H d), 7.31 ppm (1H d), 7.26 ppm (1H t), in ¹H NMR spectrum of AA (Fig. S5), the peaks were observed at $\delta = 6.67$ ppm (4H d), 7.32 ppm (2H s), and 7.94 ppm (1H s), and in ¹H NMR spectrum of IMC (Fig. S6), the peaks were observed at $\delta = 13.72$ ppm (1H s), 13.04 ppm (1H s), 8.63 ppm (1H s), 6.86 ppm (4H t); region $\delta = 8.5$ to 7.30 ppm indicates aromatic protons. The peaks of carboxylic protons, $\delta = 11.41$ ppm of NBA and $\delta = 7.94$ ppm of AA of both parent components, appeared with shifted $\delta = 13.72$ ppm and 13.04 ppm in IMC spectrum, suggesting thereby the formation of a new IMC.

Fig. 3 Powder X-ray diffraction pattern of AA, NBA, their eutectics, and the cocrystal

Enthalpy of fusion

The idea about the structure of eutectic melt and the nature of interaction between the two components forming the eutectics and the IMC could be obtained from the knowledge of their enthalpy of fusion values. The DSC plots of the pure components, the eutectics, and the IMC are given in Fig. 2. The IMC and both eutectics are showing only one peak in their DSC spectra due to their melting points, and both parent compounds show one additional peak before their melting which may be due to any kind of phase transition because both compounds have intramolecular hydrogen bonding. For the purpose of comparison, the experimental values of enthalpy of fusion and the values that are computed using the mixture law [21] are included in Table 1. The value of enthalpy of mixing, which is the difference between the experimental and the calculated values of heat of fusion, is negative, suggesting thereby a clustering of molecules for both binary eutectic melts [22]. The entropy of fusion ($\Delta_{\text{fus}}S$) of the pure components, the eutectics, and the addition compound can be calculated using the equation:

$$\Delta_{\text{fus}}S = \frac{\Delta_{\text{fus}}H}{T}, \quad (2)$$

where T is the melting temperature and ΔH is the value of enthalpy of fusion of the compound. The values of the entropy of fusion (Table 1) being positive suggest that there is increase in randomness of the system during melting as expected. The enthalpy of fusion values also influences the critical radius and interfacial energy. When a melt is cooled below its equilibrium melting temperature, the liquid phase does not solidify spontaneously because, under equilibrium condition, it contains a cluster of molecules. So long as the clusters are all below the critical size [23], they cannot grow to form crystals and, therefore, no solid would result. The interfacial energy (σ) is related to the critical size (r^*) of the nucleus according to the following equation:

$$r^* = \frac{2\sigma T_{\text{fus}}}{\Delta_{\text{fus}}H \cdot \Delta T} \quad (3)$$

where T_{fus} , $\Delta_{\text{fus}}H$, and ΔT are melting temperature of eutectic, heat of fusion, and degree of undercooling, respectively. The interfacial energy is given by the expression:

$$\sigma = \frac{C \cdot \Delta_{\text{fus}}H}{(N_A)^{1/3} (V_m)^{2/3}}, \quad (4)$$

where N_A is the Avogadro number, V_m is the molar volume, and parameter C lies between 0.30 and 0.35. The interfacial energies of pure components and eutectics were calculated by making use of enthalpy of fusion data and are

reported in Table 1. It is evident that the value of interfacial energy in case of AA is the maximum and it is the minimum in case of NBA. Other values are in between these two limits. This suggests that the role of interfacial energy is the maximum in case of AA and it is the minimum in case of NBA in the formation of the critical nucleus.

Excess thermodynamic functions

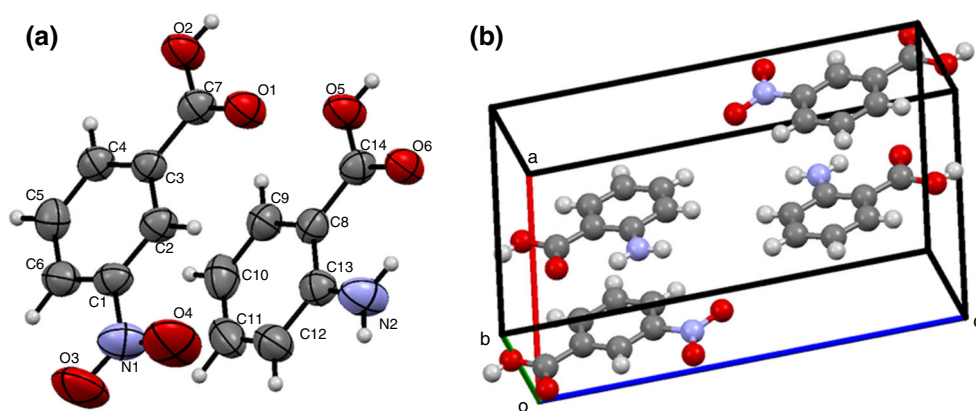
A measure of deviation from ideal behavior can be best expressed in terms of excess thermodynamic functions, namely excess free energy (g^E), excess enthalpy (h^E), and excess entropy (s^E), which give a more quantitative idea about the nature of molecular interactions. The excess thermodynamic functions (Y^E) are defined as the difference between the thermodynamic functions of mixing for a real system and the corresponding values for an ideal system at the same temperature and pressure. Thus,

$$Y^E = \Delta Y_{\text{mix}}(\text{real}) - \Delta Y_{\text{mix}}(\text{ideal}), \quad (5)$$

Table 3 Crystal data and details of the refinement for the cocrystal

	NBA-AA
Formula	C ₁₄ H ₁₂ N ₂ O ₆
M_r	304.26
CCDC No.	1422766
Crystal system	Triclinic
Space group	$P - 1$
$a/\text{\AA}$	7.4707(14)
$b/\text{\AA}$	7.6082(14)
$c/\text{\AA}$	14.171(3)
$\alpha/^\circ$	87.188(16)
$\beta/^\circ$	79.897(16)
$\gamma/^\circ$	61.105(19)
$V/\text{\AA}^3$	693.7(3)
Z	2
$D_{\text{calcd}}/\text{g cm}^{-3}$	1.457
μ (MoK α)/mm ⁻¹	0.116
$F(000)$	316.00
hkl range	$\pm 10, \pm 10, - 18/19$
T/K	298
Reflections measured	5322
Reflections unique	3135
Data with $F_o > 4\sigma(F_o)$	1419
R_{int}	0.0403
Parameters refined	397
$R(F)$ (for $F_o > 4\sigma(F_o)$)	0.0895
$wR(F2)$ (all reflections)	0.2697
GoF ($F2$)	1.029

Fig. 4 **a** ORTEP view and numbering scheme and **b** unit cell diagram of the cocrystal



where Y is any of the excess thermodynamic functions. The excess thermodynamic functions could be calculated using the thermodynamic equations reported earlier [24–26], and the values are given in Table 2. The positive values of excess free energy indicate that the interaction between the like molecules (NBA–NBA and IMC–IMC) is stronger than the interaction between the unlike molecules (NBA–IMC) in case of E_1 and in case of E_2 , interaction between AA–AA and IMC–IMC is stronger than the interaction between the unlike molecules (AA–IMC) [26].

X-ray diffraction studies

Powder X-ray diffraction patterns of parent components (AA and NBA) and their eutectics and IMC were recorded at room temperature and are depicted in Fig. 3. It is evident from the figure that the XRD pattern of IMC is quite different from either component. X-ray diffraction patterns of IMC show some new peaks which could not be assigned for either of the parent components. The intensity of some of the peaks of the parent compounds has shown significant changes in it. This observation confirms the formation of IMC (a new compound) [27]. The powder XRD pattern of

the E_1 shows the peaks of the IMC and NBA, whereas the E_2 shows the presence of X-ray peaks of the IMC and AA. These observations confirm that the eutectic E_1 is mechanical mixture of NBA and IMC and eutectic E_2 is the mechanical mixture of IMC and AA. For eutectic E_1 , the X-ray peak of AA could not be assigned, and similarly for eutectic E_2 , the peaks of NBA cannot be assigned; rather, we could assign the peaks of IMC in both eutectics from which it can be inferred that IMC behaves as a parent component for both the eutectics. The experimentally generated powder XRD pattern of the cocrystal from its single-crystal XRD data (Fig. S7) was found to be almost same as the powder XRD pattern of the IMC.

Single-crystal X-ray diffraction of the cocrystal

The single crystal of the cocrystal was grown from the saturated solution of methanol using slow evaporation technique at room temperature. A yellowish transparent single crystal was selected for X-ray diffraction and analysis. From the single-crystal X-ray diffraction analysis of the crystal, it can be inferred that it has been crystallized as cocrystal in monoclinic unit cell with $P - 1$ space group. The lattice parameters as well as various other

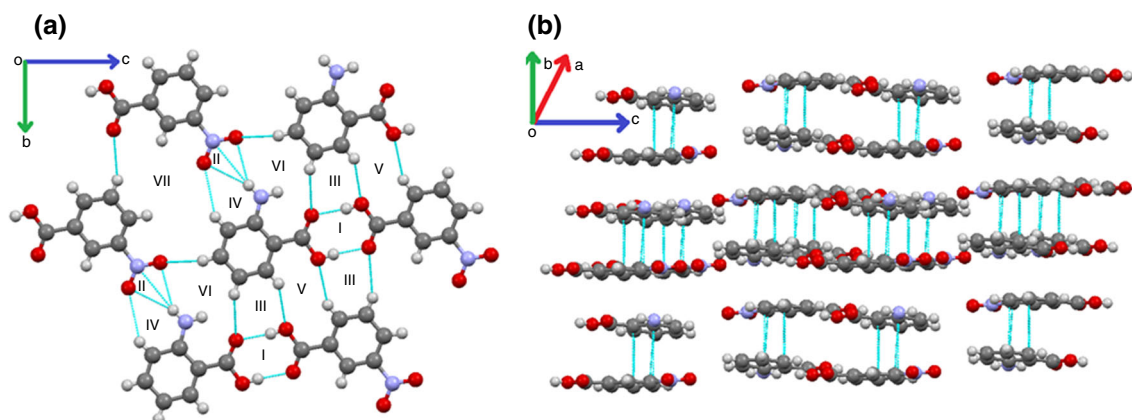
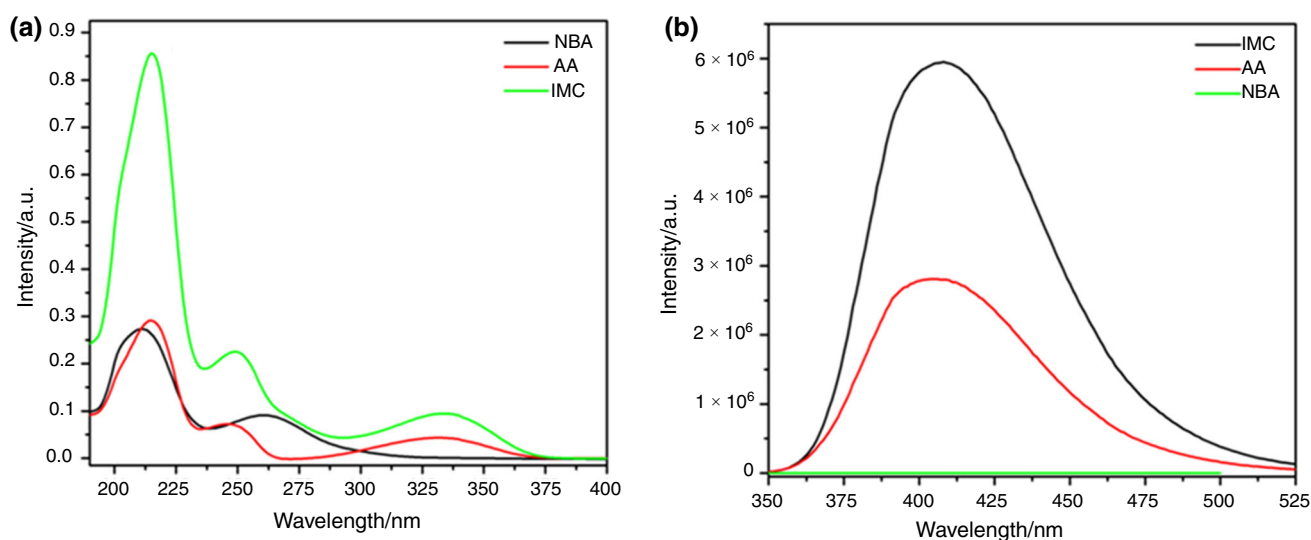


Fig. 5 Packing diagram. **a** different synthonic interactions along bc plane and **b** π - π stacking along the diagonal of ab plane in the cocrystal

Table 4 Hydrogen bond parameters (\AA and $^\circ$) in the cocrystal

Symmetry code	Interactions	Geometry		
		D...A/ \AA	H...A/ \AA	D-H...A/ $^\circ$
x, y, z	N2-H2B...O6	2.712	1.96	125
$-x, -y + 1, -z$	C4-H4...O5	3.449	2.52	143
	C9-H9...O2	3.436	2.59	135
	C4-H4...O2	3.568	2.90	121
$x - 1, +y + 1, +z$	C5-H5...O1	3.643	2.66	152
	C10-H10...O6	3.615	2.68	145
$-x, -y + 1, -z - 1$	C11-H11...O3	3.429	2.49	145
	C6-H6...O3	3.529	2.90	117
$-x + 1, -y, -z - 1$	N2-H2A...N1	3.713	2.69	172
	N2-H2A...O3	3.266	2.36	146
	N2-H2A...O4	3.361	2.37	160
	C12-H12...O4	3.600	2.66	145
$-x + 1, -y, -z$	O2-H2C...O5	3.582	2.86	135
	O2-H2C...O6	2.613	1.68	175
	O5-H5A...O1	2.647	1.71	174
	O5-H5A...O2	3.582	2.86	135

**Fig. 6** **a** UV-Vis absorption spectra, **b** emission spectra of AA, NBA, and their cocrystal

crystallographic data of the cocrystal are given in Table 3. The selected bond length and bond angle between different atoms of the cocrystal are given in Table [S2] and Table [S3], respectively. The ORTEP view and numbering scheme of cocrystal are shown in Fig. 4a, and unit cell diagram is given in Fig. 4b. The cocrystal of NBA and AA is bonded via intermolecular hydrogen bonding. The asymmetric unit of cocrystal consists of one AA and one NBA in 1:1 molar ratio. The cocrystal shows synthonic interactions (in bc plane, Fig. 5a), in which $-\text{COOH}$ group of NBA is bonded with $-\text{COOH}$ group of AA (synthon I, Fig. 5a) via $\text{O}\cdots\text{H}-\text{O}$ and $\text{O}\cdots\text{H}-\text{O}$ strong hydrogen bonding and $-\text{NO}_2$ group of NBA is bonded with $-\text{NH}_2$ group of

other AA (synthon II, Fig. 5a) via $\text{O}\cdots\text{H}-\text{N}$ and $\text{N}\cdots\text{H}-\text{N}$ hydrogen bonding. The cocrystal is also having $\text{O}\cdots\text{H}-\text{C}$ intermolecular interaction between aromatic H-atom of NBA and synthon I of other molecular pair (synthon III, Fig. 5a). The other synthons IV, V, VI, and VII (Fig. 5a) are the consequences of synthons I, II, and III. In addition to these interactions, the cocrystal also has $\pi-\pi$ stacking (3.352 \AA) between two layers (which have synthonic interactions) along the diagonal of ab plane (Fig. 5b). The H-bonding distance parameters are tabulated in Table 4.

Optical study of AA, NBA, and their IMC

UV–Vis spectrum of NBA shows two bands one an intense peak at 210 nm due to $n \rightarrow \sigma^*$ transition and the other band at 262 nm of comparatively low intensity due to $\pi \rightarrow \pi^*$ transition. AA shows three bands at 215, 249, and 332 nm due to $n \rightarrow \sigma^*$, $\pi \rightarrow \pi^*$, and $n \rightarrow \pi^*$ transitions, respectively, in decreasing order of intensity. The IMC does not show any additional peak, but it retains three bands of AA with an increase in absorption intensity (Fig. 6a). It is in accordance with hyperchromic transitions which are sensitive to hydrogen bonding [28]. AA shows emission in 355–515 nm range on σ_{\max} excitation, and NBA does not show any emission on σ_{\max} excitation. The IMC also shows a broad emission band from 355 to 525 nm with 13.2% quantum yield on excitation at σ_{\max} absorption (332 nm) in comparison with pyrene emission, which is more than twice of the AA (Fig. 6b). The increment of quantum yield of the IMC is due to extension of conjugation [29].

Conclusions

The phase diagram study on AA–NBA system shows the formation of 2:1 (NBA:AA) inter-molecular complex (IMC) with congruent melting point and two eutectics (E_1 at 0.084 and E_2 at 0.917 mol fraction of AA) on either side of the IMC. The spectroscopic studies suggest the formation of hydrogen bonding between AA and NBA which yield their polycrystalline materials known as IMC. The values of heat of mixing (-3.88 for E_1 and -5.49 kJ Mole $^{-1}$ for E_2) suggest the clustering of molecules for both eutectics, while the study of excess free energy (0.2547 for E_1 and 0.2421 kJ Mole $^{-1}$ for E_2) reveals the favored molecular associations between unlike molecules in the eutectic melt. The UV–Vis spectra of IMC show the hyperchromic effect with respect to AA and NBA. A single crystal in 1:1 molar ratio was crystallized as cocrystal in the triclinic crystal system with $P-1$ space group, and it is cocrystal of AA and NBA, which retains the identity of functional group of parent components. The cocrystal shows different synthonic interactions having $O \cdots H-O$, $O \cdots H-N$, and $N \cdots H-N$ strong hydrogen bonding, between both parent compounds along with $\pi-\pi$ staking (3.352 Å).

Acknowledgements Authors thank the University Grant Commission (UGC), India, and BHU for financial support to MS.

References

- Sangster J. Phase diagrams and thermodynamic properties of binary organic systems based on 1,2-,1,3-,1,4-diaminobenzene or benzidine. *J Phys Chem Ref Data*. 1994;23(2):295–338.
- Rai RN, Reddi RSB, Rai US. Developments and future directions of phase diagram, physicochemical and optical studies of binary organic complexes. *Prog Cryst Growth Charact Mater*. 2013;59(2):73–111.
- Okumuş M. Thermal characterization of binary mixture of some supramolecular liquid crystals. *J Therm Anal Calorim*. 2015;120(3):1603–8.
- Rai US, Singh M. An overview of the progress in solidification of binary monotectics. *J Mater Chem Eng*. 2013;1(2):75–84.
- Singh NB, Agrawal T, Gupta P, Das SS. Solidification behavior of the benzamide + O-chlorobenzoic acid eutectic system. *J Chem Eng Data*. 2009;54(5):1529–36.
- Chem YP, Tang M, Cuo TC. Solid–liquid equilibria for binary mixtures of *N*-phenylacetamide with 4-aminoacetophenone, 3-hydroxyacetophenone and 4-hydroxyacetophenone. *Fluid Phase Equilib*. 2005;232(2):182–8.
- Rai RN, Ramasamy P, Lan CW. Synthesis and crystal growth of binary organic NLO material UNBA. *J Cryst Growth*. 2002;235(1):499–504.
- Horiuchi S, Tokura Y. Organic ferroelectrics. *Nat Mater*. 2008;7(5):357–66.
- Horiuchi S, Kumari R, Tokura Y. A supramolecular ferroelectric realized by collective proton transfer. *Angew Chem Int Ed*. 2007;46(19):3497–501.
- Abbott AP, Taib KE, Frisch G, Ryder KS, Weston D. The electrodeposition of silver composites using deep eutectic solvents. *Phys Chem Chem Phys*. 2012;14(7):2443–9.
- Sechiguchi K, Obi N. Studies on absorption of eutectic mixture. I. A comparison of the behavior of eutectic mixture of sulfathiazole and that of ordinary sulfathiazole in man. *Chem Pharm Bull*. 1961;9(11):866–72.
- Cherukuvada S, Nangia A. Eutectics as improved pharmaceutical materials: design, properties and characterization. *Chem Commun*. 2014;50(8):906–23.
- Springwl G, Norberg B, Robeyns K, Wouters J, Leysess T. Advances in pharmaceutical co-crystal screening: effective co-crystal screening through structural resemblance. *Cryst Growth Des*. 2012;12(1):475–84.
- Desiraju GR. Supramolecular synthons in crystal engineering—a new organic synthesis. *Angew Chem Int Ed Engl*. 1995;34:2311–27.
- Fan E, Vincent C, Geib SJ, Hamilton AD. Molecular recognition in the solid state: hydrogen-bonding control of molecular aggregation. *Chem Mater*. 1994;6:1113–7.
- Dean JA. Lange's handbook of chemistry. New York: McGraw-Hill; 1985.
- Singh M, Rai RN, Rai US. Synthesis, crystal growth and physicochemical studies on a novel organic inter-molecular compound; 3,5-dinitrobenzoic acid and salicylamide system. *J Cryst Growth*. 2015;419:114–22.
- Reddi RSB, Kant S, Rai US, Rai RN. Crystallization, thermal, phase diagram and microstructural studies of organic analog of metal–nonmetal monotectic alloy: 4-bromochlorobenzene–succinonitrile. *J Cryst Growth*. 2009;312:95–9.
- Sheldirck GM. Shelex-97, program for crystal structure refinement from diffraction data. Göttingen: University of Göttingen; 1997.
- Rai US, Singh M, Rai RN. Solid state synthesis, structural, physicochemical and optical properties of an inter-molecular

- compound: 2-hydroxy-1,2-diphenylethanone-4-nitrophenylenediamine system. *J Solid State Chem.* 2017;253:63–72.
21. Rai RN, Verma KBR. Phase diagram and dielectric studies of binary organic materials. *Mater Lett.* 2000;44:284–93.
 22. Singh M, Rai US, Rai RN. Some physicochemical and thermal studies on organic analog of a nonmetal-nonmetal monotectic alloy; 2-cyanoacetamide–4-chloronitrobenzene system. *Am J Anal Chem.* 2011;2:953–61.
 23. Reddi RSB, Ganesamoorthy S, Gupta PK, Rai RN. Phase equilibria, crystallization, thermal and microstructural studies on organic monotectic analog of nonmetal–nonmetal system; urea–4-bromo-2-nitroaniline. *Fluid Phase Equilib.* 2012;313:121–6.
 24. Rai US, Singh M, Rai RN. Some physicochemical studies on organic eutectics and intermolecular compounds. *J Therm Anal Calorim.* 2017. <https://doi.org/10.1007/s10973-017-6429-7>.
 25. Reddi RSB, Kumar Satuluri VSA, Rai US, Rai RN. Thermal, physicochemical and microstructural studies of binary organic eutectic systems. *J Therm Anal Calorim.* 2012;107:377–85.
 26. Reddi RSB, Kumar Satuluri VSA, Rai RN. Solid–liquid equilibrium, thermal and physicochemical studies of organic eutectics. *J Therm Anal Calorim.* 2012;107:183–8.
 27. Rai US, Singh M, Rai RN. Green synthesis, characterization and some physico-chemical studies on a novel intermolecular compound; 4-nitro-phenylenediamine-*N,N*-dimethylaminobenzaldehyde system. *J Mol Struct.* 2017;1144:41–8.
 28. Kalsi PS. Spectroscopy of organic compounds. 6th ed. India: New Age Publication; 2005.
 29. Naumov P, Ohashi Y. Packing-dependent photochromism: the case of photoinduced intramolecular proton transfer in 6-(2',4'-dinitrobenzyl)-2,2'-bipyridine. *Acta Cryst.* 2004;B60:343–9.